Ceramics International **21** (1995) 181–186

Sintering Development and Oxidation Characterization of $AlYO_3$-Doped Si_3N_4 Ceramic

Chih-Hung Yeh & Min-Hsiung Hon

Department of Materials Science and Engineering (MAT32), National Cheng Kung University, Tainan, Taiwan

(Received 21 December 1993; accepted 9 March 1994)

Abstract: The liquid phase sintering development and oxidation characterization of Si_3N_4 ceramic with $AlYO_3$ and equimolar Y_2O_3 + Al_2O_3 as sintering aids, respectively, have been studied. The apparent onset densification temperature and the shrinkage rate were recorded by dilatometer in sintering. The strength dependence and phase evolution for both $AlYO_3$-doped and Al_2O_3 + Y_2O_3-doped Si_3N_4 ceramics oxidized at temperature range from 700 to 1000°C for 100 h are analyzed. Specimens oxidized at 850°C for 100 h can improve the flexure strength due to the formation of an oxide products layer possibly sealing off surface pores.

1 INTRODUCTION

Because of the high degree of covalent bonding, classical sintering is not used to produce dense Si_3N_4 ceramics. As a consequence, the addition of sintering aids, such as Y_2O_3 and Y_2O_3 + Al_2O_3[1–5] to Si_3N_4 powders which react with SiO_2 (always introduced on the surface of Si_3N_4 powders during its synthesis process) and then create liquid-phase sintering assisting the densification. However, inhomogeneous mixing between separate powders Y_2O_3 + Al_2O_3 and Si_3N_4 always exists. The formation of liquids with different compositions and viscosities, such as Al_2O_3-rich liquid with lower viscosity enhancing local densification and Y_2O_3-rich liquid with higher viscosity[6] delaying local densification, might result in non-uniform densification and finally a non-uniform microstructure. Therefore, in order to achieve a higher homogeneity of the Y_2O_3 + Al_2O_3 addition within the Si_3N_4 powders, some investigators used yttrium aluminates, such as $AlYO_3$ and $Al_5Y_3O_{12}$,[7–10] as sintering aids replacing separate powders Y_2O_3 + Al_2O_3. Kuziukevics and Ishizaki[7] compared the difference of Si_3N_4 sintering with $AlYO_3$ and equimolar mixtures of Y_2O_3 + Al_2O_3 as sintering aids. It was indicated that the $AlYO_3$ as sintering additive for Si_3N_4 has a better densification capability than Y_2O_3 + Al_2O_3 at temperatures above 1700°C, and suggested that is due to the heterogeneity of liquid phase formation in the case of using Y_2O_3 + Al_2O_3 as sintering aid. However, they did not investigate the development of densification behaviors in $AlYO_3$-doped Si_3N_3 systems.

In an attempt to intensively compare the development of liquid-phase sintering behavior of Si_3N_4 ceramics with $AlYO_3$ and separated powder mixtures Al_2O_3 + Y_2O_3 as sintering aids, this work observes their densification shrinkage profiles, not only in pressureless sintering, but also in hot pressed sintering by dilatometer. Also, the mechanical properties and phase development in oxidation are also discussed in terms of additive compositions.

2 EXPERIMENTAL PROCEDURE

Yttrium aluminate ($AlYO_3$) was prepared from the powder mixtures of Al_2O_3 (99·99%, AKP-50, Sumitomo Co. Ltd., Japan) and Y_2O_3 (99·9%, Research Chemicals, USA) of molar ratio Al_2O_3/Y_2O_3 = 1/1 calcined at 1600°C for 4 h and then crushed. The resultant powder was calcined again at 1700°C for 2 h and then crushed and

Ceramics International 0272-8842/95/$9.50. Printed in Great Britain

Table 1. Compositions and sintering conditions of specimens

Specimen series	Composition wt(%) Si_3N_4	Al_2O_3	Y_2O_3	$AlYO_3$	Sintering condition Temperature (°C)	Furnace	Time (h)
PR10	90	3·11	6·89	—	1750	PLS	2
HPR10	90	3·11	6·89	—	1750	HP	1
PC10	90	—	—	10	1750	PLS	2
HPC10	90	—	—	10	1750	HP	1
PR6	94	1·87	4·13		1750	PLS	2
PC6	94	—	—	6	1750	PLS	2

PLS: pressureless sintering; HP: hot-press sintering.

ball-milled to control its average particle size to within 5 μm. Complete reaction was confirmed by X-ray analysis. Si_3N_4 powder (SN-E10, particle size 0·3 μm, specific surface area 11·2 m^2/g, alpha content 95 wt%, UBE Chemical Co. Ltd., Japan) was mixed with 6 and 10 wt% of additives for the Al_2O_3–Y_2O_3 and $AlYO_3$ systems, respectively (Table 1), in ethanol by ball-milling for 24 h, using silicon nitride media. The slurry was dried by vacuum filter drying to eliminate solvent, then placed in an oven at 90°C for 24 h. The obtained powder was crushed and sieved through 80-mesh screen, then uniaxially pressed at a pressure of 20 MPa to make pellets of 15 mm diameter and 3 mm height and 55 × 5 × 4 mm bars. The compacts were cold isostatically pressed at 250 MPa for 1 min. The as-cipped specimens were pressureless sintered at 1750°C for 2 h in 1 atm N_2 (high purity grade) using a graphite furnace. In order to prevent decomposition of Si_3N_4 in the sintering process, the green compacts were embedded in a powder bed with compositions of 60 wt% (Si_3N_4 + additives)–40 wt%BN. Shrinkage profiles in sintering were determined using a high temperature dilatometer (DHT 2050 type, Setaram, France). Hot pressed sintering was performed using a graphite furnace (FVPHP-R-5, Fujidempa, Japan) in 1 atm flowing N_2 at 1750°C for 1 h with a pressure of 25 MPa. The hot pressing variables, such as time, temperature, pressure, and ram displacement, were recorded. Density of the sintered specimens was measured using the water immersion method. The oxidation was carried out in air temperatures from 700 to 1000°C for 100 h. Flexural strength measurement was performed using a three-point bending method with a span of 30 mm and a crosshead speed of 0·5 mm/min. The Vickers hardness and fracture toughness were measured by the Vickers indentation method with a load of 50 kg. The phase identification was determined by powder X-ray diffraction analysis (XD-D1, Shimadzu, Japan). The scanning electron microscope (JSM-5200, JEOL, Japan) was employed for the morphological examination of the fracture and etched surface.

3 RESULTS AND DISCUSSION

3.1 Sintering development

Figure 1 shows the densification shrinkage profiles of pressureless-sintered Si_3N_4 as a function of temperature and additive compositions. The apparent onset densification temperature (T_s) is obtained from the shrinkage curves at 1330°C and 1390°C for specimens PR10 and PC10 (Table 1), respectively, which is attributed to the formation of an eutectic melt causing the viscous flow and then providing the driving force for particle rearrangement. The difference of T_s values between specimens PR10 and PC10 can be explained by referring to the possible eutectic formation temperature in SiO_2–Al_2O–Y_2O_3–Si_3N_4 liquid which is lower than that in SiO_2–$AlYO_3$–Si_3N_4 liquid. The eutectic temperature in Y_2O_3–Al_2O_3–SiO_2 triangle is at 1345°C.[11] Apparently, it is near to onset densification temperature, T_s, in Al_2O_3 + Y_2O_3-doped

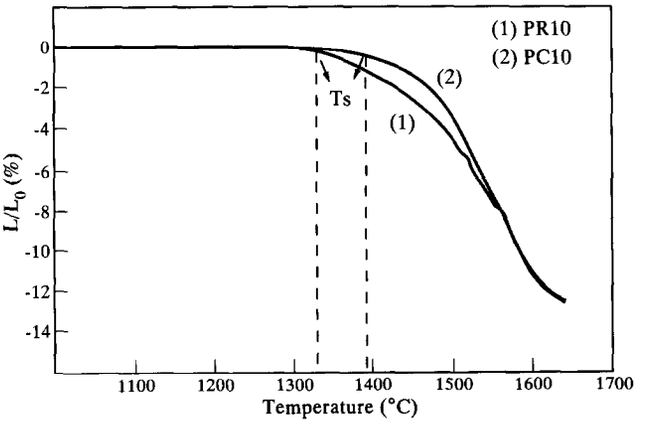

Fig. 1. Shrinkage dependence on heated temperature for specimens PR10 (10 wt% Al_2O_3 + Y_2O_3 addition) and PC10 (10 wt% $AlYO_3$ addition).

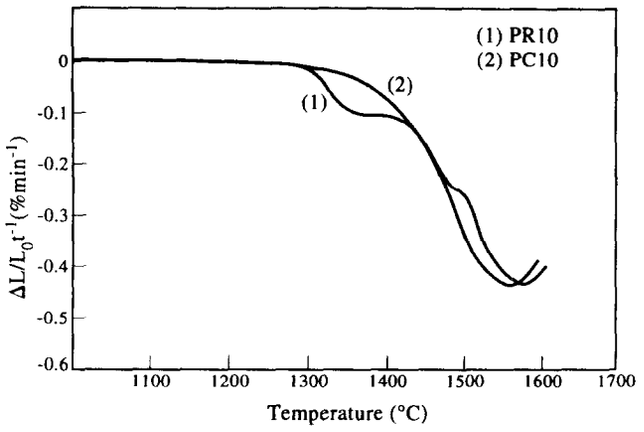

Fig. 2. Shrinkage rate curves of specimens PR10 and PC10.

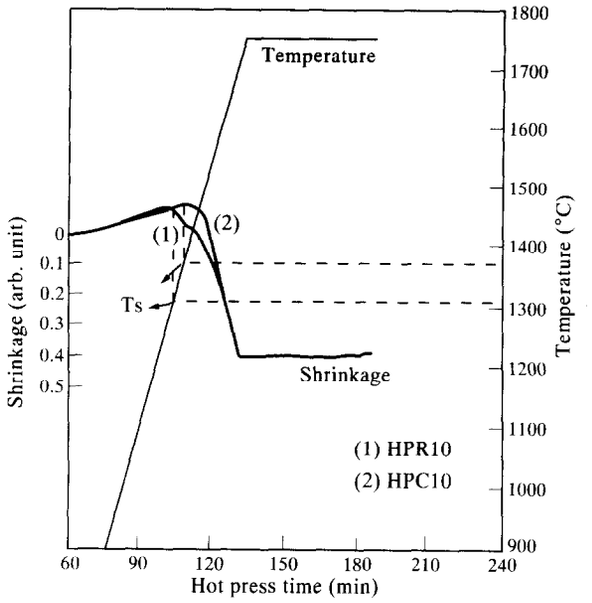

Fig. 3. Heating temperature and specimens shrinkage in hot-pressing.

Si_3N_4 systems. $AlYO_3$ is stable in the temperature range from 1820°C to 1900°C,[12] however, the possible decomposition and reaction with SiO_2 at sintering temperature are still not clear.

The temperature dependence of shrinkage rate, $(\Delta L/L_0)t^{-1}$, in Fig. 2 shows that the maximum shrinkage rate occurs at 1560°C and 1580°C for specimens PC10 and PR10, respectively. Also, Si_3N_4 with $AlYO_3$ additive, for PC10 specimen, was densified with a faster rate than the one with Al_2O_3 + Y_2O_3 mixtures, PR10 specimen at temperature above 1460°C. For liquid phase sintering, the densification during rearrangement and solution–diffusion–reprecipitation are closely related to the viscosity of the liquid phase. In general, the decreased viscosity of the liquid phase during sintering will promote the densification (i.e. increasing shrinkage rate).[13,14] As a consequence, the enhanced shrinkage rate for specimen PC10 may be due to the decreased viscosity of the liquid and then accelerates the rearrangement and solution–diffusion–reprecipitation mechanisms for densification.

Figure 3 shows the shrinkage curves of hot-press sintered Si_3N_4 as a function of temperature and additive compositions. The T_s is observed at 1315°C for specimen HPR10, higher than that for specimen HPC10 (1370°C). Also, the T_s of all the specimens with the same composition in hot-press sintering are lower than that in pressureless sintering. This is due to the external stress provided from mechanical pressing in hot-press sintering which promotes the particle rearrangement. Obviously, the densification rate, namely the slope of shrinkage curves vs sintering time, for specimen HPC10 is faster than that of specimen HPR10 at temperatures above 1450°C giving the same results as listed of pressureless sintering.

Table 2 summarizes the results of relative density and room temperature mechanical properties of sintered Si_3N_4. The dependence of relative density and mechanical properties is associated with the amount and compositions of additives, as well as sintering conditions. In the case of Si_3N_4 with 10 wt% $AlYO_3$ addition, specimens PC10 and HPC10 obtained higher relative density, flexure strength and Vickers hardness than specimens PR10 and PC10 with 10 wt% equimolar Al_2O_3 + Y_2O_3 mixture added. To compare the specimens containing 10 wt% and 6 wt% additives, specimens PR6 and PC6 exhibit poor sinterability and mechanical properties. Also, among specimens PR6 and PC6, the latter still obtains a higher relative density.

Table 2. The summarized results of relative density and room temperature mechanical properties of sintered Si_3N_4

Specimen series	Relative density (%)	$\beta(Si_3N_4)$ $\alpha(Si_3N_4)$ (%)	σ (MPa)	Hv (GPa)	K_{IC} (MPa m$^{1/2}$)
PR10	97·1	98	749±64	14·9±0·4	7·7
PC10	98·2	99	813±32	15·0±0·7	7·3
PR6	93·4	—	693±63	12·1±1·2	6·9
PC6	94·3	—	661±59	13·0±08	6·3
HPR10	99·8	—	940±42	15·9±02	5·5
HPC10	99·9	—	1052±37	16·3±02	5·4

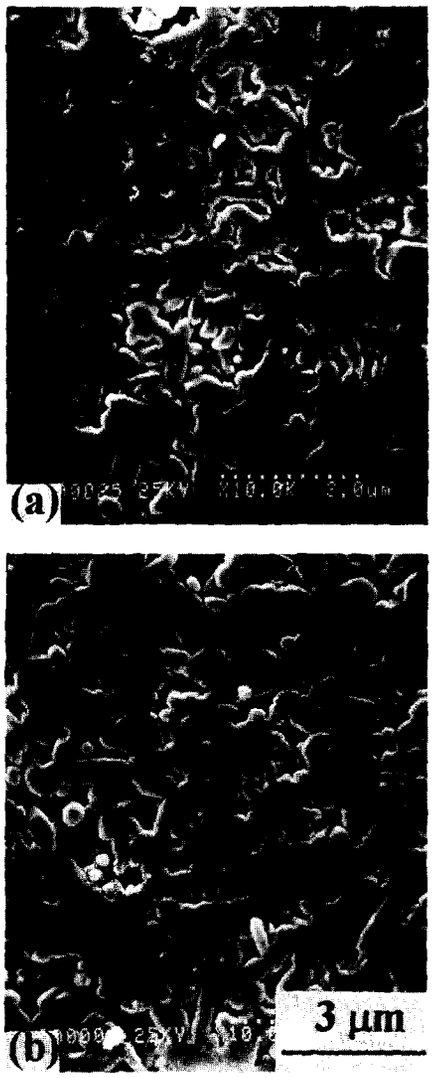

Fig. 4. Typical microstructures of specimens (a) PC10 and (b) PR10 etched in a molten alkali hydroxide with a composition of NaOH:KOH = 1:1 at 450°C for 10–15 s.

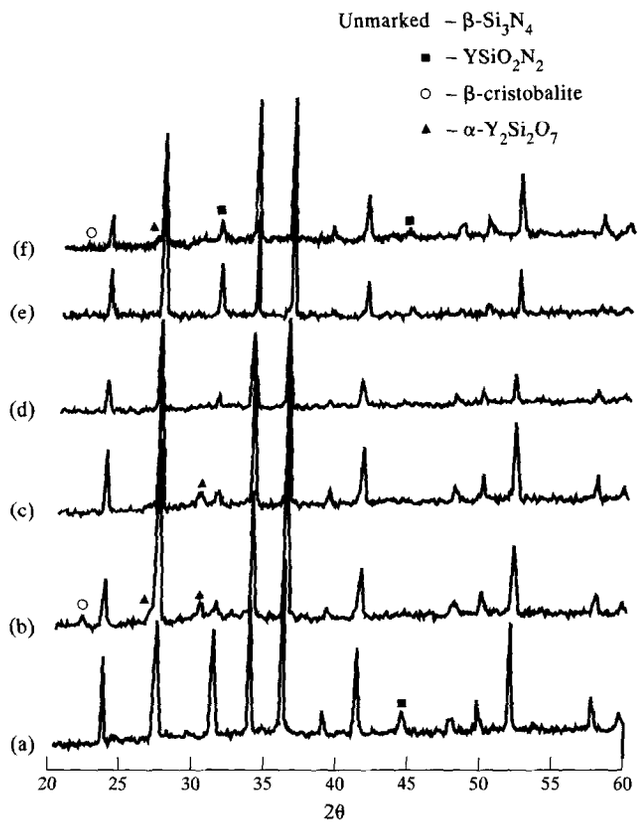

Fig. 5. X-Ray diffraction patterns of Si_3N_4 ceramics with 10 wt% additives added before and after oxidation at 1000°C for 100 h. (a) PC10 unoxidized, (b) PC10 oxidized, (c) with a layer of 2 × 10^{-2} mm in thickness ground off, and (d) with a layer 4 × 10^{-2} mm in thickness ground off, (e) PR10 unoxidized, and (f) PR10 oxidized.

The SEM micrographs of the etched surface of specimens PC10 and PR10, illustrated in Fig. 4, indicated that the microstructural development of β-Si_3N_4 in both specimens is similar. An average grain size of approximately 0·5 μm in width and 2–3 μm in length is estimated in these specimens using the quantitative microstructural characterization method.[11]

3.2 Characterization of oxidized Si_3N_4 ceramics

Figure 5 is an XRD study of the phase evolution of specimens PC10 and PR10 before and after oxidation at 1000°C for 100 h. Both specimens (PC10 and PR10) contain β-Si_3N_4 and $YSiO_2N_2$ crystalline phases. The oxidized surface of PC10 consists of β-Si_3N_4, remnant $YSiO_2N_2$ and oxidation products, α-$Y_2Si_2O_7$ and β-cristobalite. With different results to specimen PC10, the oxidized surface of specimen PR10 mainly includes β-Si_3N_4 and $YSiO_2N_2$ and only minor β-cristobalite and α-$Y_2Si_2O_7$ diffraction peaks can be detected. As the oxidized surface of specimen PC10 is ground out, layers with thickness of 2 × 10^{-2} mm and 4 × 10^{-2} mm, respectively, the β-cristobalite and α-$Y_2Si_2O_7$ diffraction peaks disappear. Figure 6 is the XRD of specimens PR6 and PC6 before and after oxidation at 1000°C for 100 h. Owing to the decrease of additives added, the crystalline phase only consists of β-Si_3N_4 for both specimens PR6 and PC6. The β-cristobalite is detected only in the oxidized surface of specimen PC6, but not in specimen PR6. Some studies[15,16] have reported that the rate-determining step of Si_3N_4 ceramic oxidation is the diffusion-controlled mechanism. The XRD results seem to suggest that the presence of high diffusion path in $AlYO_3$-doped Si_3N_4 system would enhance the reaction of oxygen with Si_3N_4 ceramics on the basis of the diffusion-controlled model.

The influence of oxidation on the strength of specimens PR10 and PC10 (Fig. 7) shows a dramatic increase in the flexure strength after oxidation at 850°C for 100 h, which may be caused by an elimination of surface defects. Because the strength of Si_3N_4 ceramics is highly sensitive to surface defects and microcracks, the formation of

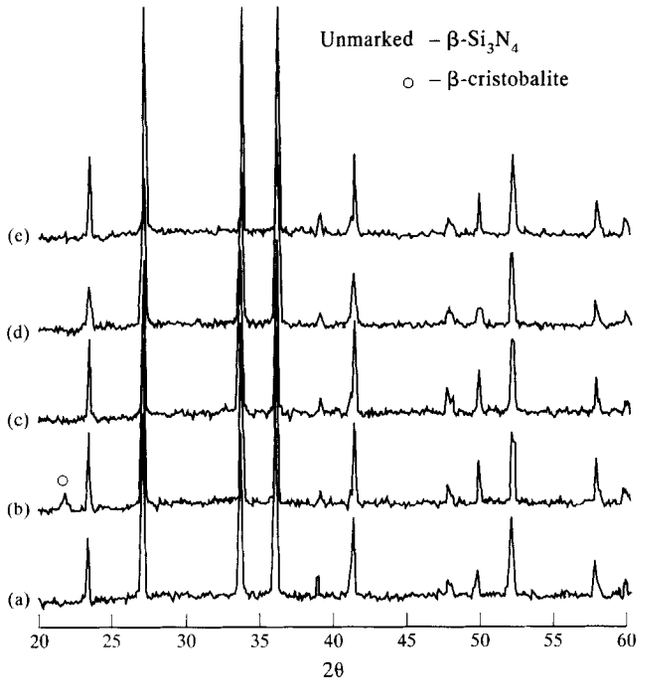

Fig. 6. X-Ray diffraction patterns of Si_3N_4 ceramics with 6 wt% additives added before and after oxidation at 1000°C for 100 h. (a) PC6 ($AlYO_3$ addition) unoxidized, (b) PC6 oxidized, (c) with a layer of 2×10^{-2} mm in thickness ground off, (d) PR6 ($Al_2O_3 + Y_2O_3$ addition) unoxidized, and (e) PR6 oxidized.

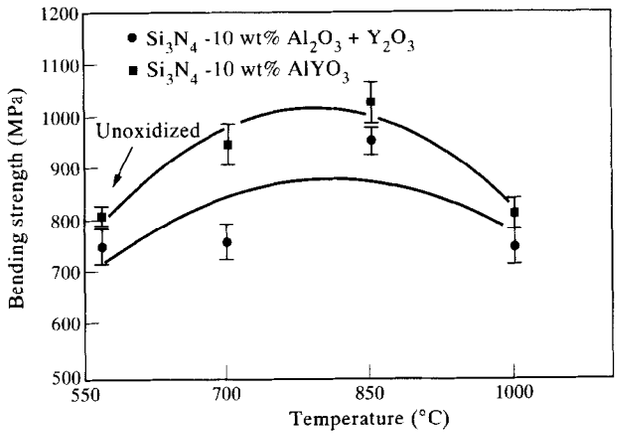

Fig. 7. Effect of oxidation temperature on the bending strength of specimens PC10 and PR10.

a thin oxide layer, resulting in the elimination of defects and blunting of microcracks, gives a positive effect on strength. The morphological examination of specimen PC10 heated at 850°C for 100 h (Fig. 8) shows that the oxidized surface is smooth and some surface pores are sealed and blunted, which provides an explanation of the strength increase after oxidation.

Figure 9 is the SEM morphology of specimen PC10 oxidized at 1000°C for 100 h. Observation of the cross-section near the oxidized surface shows that the oxide layer formed on the surface of the specimen is 2–3 μm thick. The results of XRD show that the oxidation at 1000°C induces

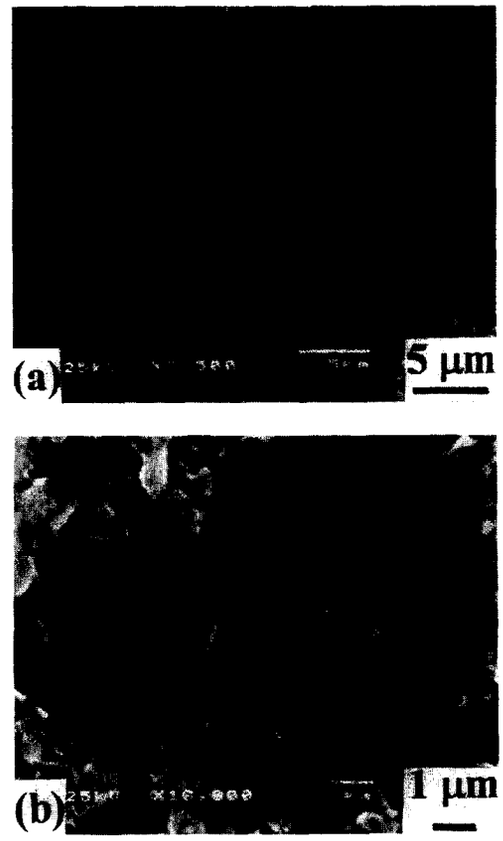

Fig. 8. SEM micrographs of oxidized surface of specimen PC10 heated at 850°C for 100 h. (a) 3·5 K, (b) 10 K.

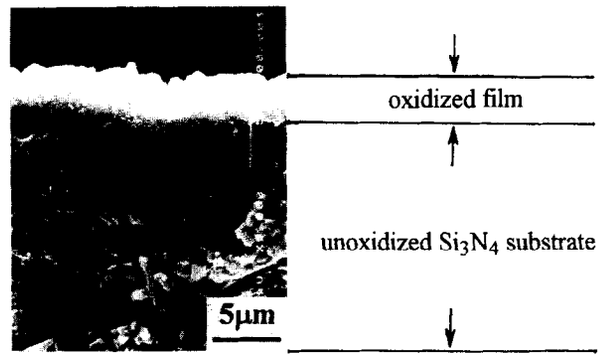

Fig. 9. SEM micrograph of the cross-section near the oxidized surface of specimen PC10 heated at 1000°C for 100 h.

the formation of yttrium silicate, α-$Y_2Si_2O_7$, by the following equation

$$YSiO_2N_2 + 0{\cdot}75\ O_2 \rightarrow 0{\cdot}5\ Y_2Si_2O_7 + N_2$$

The difference of specific molar volume between $Y_2Si_2O_7$ and $YSiO_2N_2$ leads to a 10% specific volume change,[17] which creates a build-up of stresses and gives a negative effect on strength. Therefore, after exposure at 1000°C, the strength decreases to the level of the unoxidized specimen.

4 CONCLUSION

The development and characterization of oxidized Si_3N_4 ceramics sintered with $AlYO_3$ and Y_2O_3 +

Al_2O_3 additions have been investigated. It shows that the apparent onset densification temperature for Y_2O_3 + Al_2O_3-doped Si_3N_4 ceramics is lower than that of $AlYO_3$-doped Si_3N_4 ceramics, not only in pressureless sintering but also in hot-press sintering. The densification rate for $AlYO_3$-doped Si_3N_4 ceramic is faster than that of Y_2O_3 + Al_2O_3-doped Si_3N_4 ceramic temperatures above 1460°C. Specimens oxidized at 850°C for 100 h can improve the flexure strength due to the formation of an oxide layer, possibly sealing off the pores on the specimen surface.

REFERENCES

1. HAYASHI, T. & MUNAKATA, H., Pressureless sintering of Si_3N_4 with Al_2O_3 and Y_2O_3. *J. Mater. Sci.*, **21** (1986) 3501–8.
2. LOEHMAN, R. E. & ROWCLIFFE, D. J., Sintering of Si_3N_4–Y_2O_3–Al_2O_3. *J. Am. Ceram. Soc.*, **63** (1980) 144–8.
3. ABE, O., Sintering process of Y_2O_3 and Al_2O_3-doped Si_3N_4. *J. Mater. Sci.*, **25** (1990) 4018–26.
4. QUACKENBUSH, C. L. & SMITH, J. T., Phase effect in Si_3N_4 containing Y_2O_3 or CeO_2: II Oxidation. *Ceram. Bull. (ACers)*, **59** (1980) 533–7.
5. TSUGE, A. & NISHIDA, K., High-strength hot-pressed Si_3N_4 with concurrent Y_2O_3 and Al_2O_3 additions. *Ceram. Bull. (ACers)*, **56** (1978) 424–6, 431.
6. ZIEGLER, G., HEINRICH, J. & WOTTING, G., Relationship between properties of dense and reaction-bonded silicon nitride. *J. Mater. Sci.*, **22** (1987) 3041–86.
7. KUZJUKEVICS, A. & ISHIZAKI, K., Sintering of silicon nitride with $YAlO_3$ additive. *J. Am. Ceram. Soc.*, **76** (1993) 2373–5.
8. KIM, J., SCHUBERT, H. & PETZOW, C., Sintering of Si_3N_4 with Y_2O_3 and Al_2O_3 added by coprecipitation. *J. Eur. Ceram. Soc.*, **5** (1989) 311–9.
9. LI, W. L., ZHUNG, H. R., FU, X. R. & YEN, T. S., Gas pressure sintering of RBSN with YAG addition. In *Ceramic Materials and Components for Engines*, ed. V. J. Tennery. Am. Ceram. Soc. Inc., 1988, pp. 409–18.
10. TIEGS, T., Silicon carbide-whisker-reinforced SIALON composites: Effect of sintering aid content. *Ceram. Engng Sci. Proc.*, **10** (1989) 101–7.
11. WOTTING, G., KANKA, B. & ZIEGLER, G., Microstructure development, microstructural characterization and relation to mechanical properties of dense silicon nitride. In *Non-Oxide Technical and Engineering Ceramics*, ed. S. Hampshire. Elsevier, London, 1986, pp. 83–96.
12. LEVIN, E. M., ROBBINS, C. R. & McMURDIE, H. F., *Phase Diagrams for Ceramists*, ed. M. K. Reser. Am. Ceram. Soc., 1975.
13. SARIN, V. K., On the α- to β-phase transformation in silicon nitride. *Mater. Sci. Engng*, **A105/106** (1988) 151–9.
14. PROKESOVA, M. & PANEK, Z., Particle rearrangement during liquid phase sintering of silicon nitride. *Ceram. Int.*, **15** (1989) 369–74.
15. SINGHALI, S. C., Thermodynamics and kinetics of oxidation of hot-pressed silicon nitride. *J. Mater. Sci.*, **11** (1976) 500–9.
16. LEWIS, M. H. & BARNARD, P., Oxidation mechanisms in Si–Al–O–N ceramics. *J. Mater. Sci.*, **15** (1980) 443–8.
17. PATEL, J. K. & THOMPSON, D. P., Further studies of the low-temperature oxidation problem in yttria-densified silicon nitride ceramics. In *Ceramic Materials and Components for Engines*, ed. V. J. Tennery. Am. Ceram. Soc. Inc., 1988, pp. 987–96.